30th AIAA Applied Aerodynamics Conference
25 - 28 June 2012, New Orleans, Louisiana

AIAA 2012-2797

Measurement of Unsteady Flow Reattachment on an Airfoil with a Leading-Edge Horn-Ice Shape

Phillip J. Ansell* and Michael B. Bragg†
University of Illinois at Urbana-Champaign, Urbana, Illinois 61801

A technique for identifying the unsteady shear-layer reattachment location downstream of an ice shape on an airfoil using an array of surface-mounted hot-film probes is presented. The method utilizes statistical comparison of signals from adjacent probes to identify regions of strong anti-correlation, indicating flow bifurcation at reattachment. In an example, hot-film array measurements were obtained for two airfoil models with simulated leading-edge ice shapes. These hot-film array measurements were used to generate time histories for the unsteady location of shear-layer reattachment downstream of a leading-edge ice shape. The resulting spectral content of the unsteady shear-layer reattachment locations reveal influences of regular-mode vortex shedding and shear-layer flapping. The Strouhal numbers corresponding to these two flow phenomena compared well to those found in literature. Statistical reduction of the unsteady location of reattachment is also consistent with prior work.

Nomenclature

c	=	airfoil chord length
C_p	=	coefficient of pressure
f	=	frequency
L_b	=	bubble length
L_h	=	projected height (normal to freestream)
M_∞	=	freestream Mach number
N	=	number of samples
p	=	probability density function
P	=	cumulative distribution function
r	=	time lag interval
Re	=	Reynolds number based on chord length
R_{pq}	=	cross-correlation function
St_f	=	Strouhal number corresponding to shear-layer flapping (fL_h/U)
St_r	=	Strouhal number corresponding to regular mode (fL_b/U)
U_∞	=	freestream velocity
x	=	coordinate in the airfoil model chordwise direction
x_{MR}	=	mean reattachment location
α	=	airfoil angle of attack
Δt	=	time step (inverse of sample rate)
ρ	=	cross-correlation coefficient
σ	=	standard deviation of sample
τ	=	time lag

I. Introduction

The effect of ice accretion on aircraft flight characteristics is an issue that is considered in the development of nearly all subsonic aircraft. For this reason, many past studies have been devoted to better understanding[1] and

* Graduate Research Assistant, Department of Aerospace Engineering, Member AIAA.
† Professor of Aerospace Engineering, Executive Associate Dean for Academic Affairs, Fellow AIAA.

classifying[2] traits of ice accretions, as well as to evaluate the effects of ice accretion on aircraft performance[3] and controllability.[4] However, ice-induced flowfields tend to be highly complex and affect the unsteady performance characteristics of an aircraft. For this reason, the development of diagnostic and measurement tools capable of capturing such unsteady phenomena would provide an opportunity to improve understanding of ice-induced flowfield effects.

Iced Flowfield Physics

Previous studies have shown that unsteady performance of an airfoil can be directly correlated to local flowfield features. For example, Broeren[5] displayed the existence of a quasi-periodic, low-frequency fluctuation in lift near stall that was most pronounced for airfoils with a mixed thin-airfoil/trailing-edge stall type. These fluctuations were caused by changes in the extent of the leading-edge separation bubble on the upper-surface of the airfoil.

Low-frequency changes to airfoil performance due to ice-induced flowfield effects were also investigated by Gurbacki[6] for an airfoil with a simulated horn-ice shape. The most dominant feature in the flowfield of an airfoil with a horn-ice shape is the large separation bubble that forms due to the separation off the tip of the horn-ice shape.[7] An instantaneous schematic of this separation bubble, along with some associated flowfield features, is shown in Fig. 1, after Gurbacki.[8] As shown in this schematic, the separation location occurs at the tip of the horn-ice shape. Immediately, the shear layer forms, which separates the recirculation region from the freestream flow. The shear layer begins to roll up as it moves downstream, and vortices within the shear layer merge, forming larger vortical structures. As the shear layer vortices are formed and shed, the height and length of the separation bubble tend to change as a function of time. As shown in Fig. 1, this causes the flow reattachment to occur across a range of chordwise locations downstream of the horn-ice shape.[2] It was shown by Gurbacki that the low-frequency movement of the reattachment location contributed to unsteadiness in the airfoil lift and quarter-chord pitching moment coefficients.[6]

The effect of this low-frequency movement of the shear-layer reattachment location downstream of a horn-ice shape on the unsteady flap hinge moment of an airfoil has also become an area of interest. The investigation of the effects of ice-induced flowfield features on flap hinge moment unsteadiness is unique in that it pertains to both unsteady airfoil performance as well as aircraft controllability. As shown in Ansell et al.,[9] the addition of a simulated glaze-ice accretion on an NACA 23012 model led to changes in the unsteady hinge moment behavior near stall that were distinctly different from other types of simulated leading-edge contamination configurations. Additional understanding and characterization of the unsteady shear-layer reattachment process downstream of a leading-edge glaze-ice accretion is paramount to determining these sources of unsteadiness in airfoil hinge moment near stall.

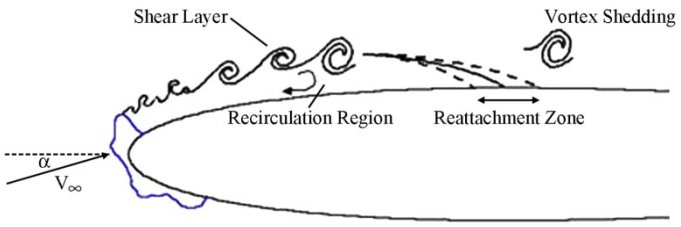

Fig. 1. Instantaneous schematic of the flowfield downstream of a horn-ice shape, after Gurbacki.[8]

The flow physics downstream of many horn-ice or spanwise-ridge-ice shapes have many similarities to the unsteady flowfield behavior downstream of a backward-facing step or a blunt flat plate. Eaton[10] determined the existence of a reattachment zone, rather than a particular reattachment line, downstream of a backward-facing step. Driver et al.[11] discovered that the separation region downstream of a backward-facing step exhibits a global "flapping" motion at a very low frequency, and also showed that most of the energy within the reattaching shear layer occurred at frequencies lower than that of turbulence, and was attributed to vortical structures. Kiya and Sasaki[12] also found the motion of vortices and a low-frequency flapping to be the two primary contributors to the unsteady motion of the reattaching shear layer. A schematic of this movement of the reattaching shear layer is shown in Fig. 2, after Kiya and Sasaki.[12] Spazzini et al.[13] also discovered a difference in spectral content of the skin-friction coefficient upstream and downstream of the mean shear-layer reattachment location downstream of a backward-facing step. These authors observed that upstream of the mean reattachment location, the spectra are primarily dominated by low-frequency fluctuations, and downstream of the mean reattachment location, contributions from both the vortex shedding and pairing process and the shear-layer flapping were visible in the skin-friction coefficient spectral content. These observations were also consistent with those by Li and Naguib,[14] who observed the low-frequency flapping to be most dominant in the shear-stress coefficient spectral content closer to the step, with increasing influence of the vortex shedding and pairing process on the spectral content of the skin-friction coefficient farther from the step.

The source of this low-frequency flapping of the shear layer is not fully understood. Kiya et al.[15] have theorized the existence of a feedback system that drives this low-frequency oscillation. This theory was also reinforced by the observations of Lee and Sung.[16] Sigurdson[17] attributed this low-frequency flapping to a parallel version of a von Kármán vortex shedding process, where an instability is generated due to the interaction of the shear-layer vorticity with its image across a wall. An alternative explanation of the source of this shear-layer flapping phenomenon is provided by Eaton and Johnston.[18] These authors believe that the low-frequency unsteadiness in the shear-layer reattachment is due to an imbalance between the rate of turbulent entrainment of fluid from the recirculation region into the separated shear layer and the rate of fluid reinjection from the reattaching shear layer into the recirculation region. Driver et al.[11] thought it to be due to a similar mechanism, consisting of a disorder of the roll-up and vortex pairing process in the shear layer.

As shown by Gurbacki,[6] the unsteady flowfield features on an airfoil with a horn-ice accretion exhibit similar classifications of spectral content as the backward-facing step flows. It was discovered that, much like the backward-facing step flow, the unsteadiness in the reattaching shear layer downstream of the horn-ice shape could be classified into a contribution from the shear-layer flapping phenomena and the regular frequency mode of vortex shedding. In this study by Gurbacki, the Strouhal number corresponding to both the shear-layer flapping phenomena (St_f) and the regular mode (St_r) were identified in agreement with those from backward-facing step flows. As also shown in Gurbacki, the Strouhal number corresponding to shear-layer flapping and the regular mode were dependent on two different length scales for non-dimensionalization.[6] In both Gurbacki[6] and Broeren,[5] the Strouhal number for the low-frequency phenomenon tended to scale with the vertical projected height of the airfoil, normal to freestream ($St_f = fL_h/U_\infty$). In contrast, in Gurbacki[6] the regular mode tended to scale with the length of the separation bubble ($St_r = fL_b/U_\infty$). For a 2D extrusion of a horn-ice shape, the range of Strouhal numbers observed by Gurbacki were $St_f = 0.00487\text{-}0.01023$, and $St_r = 0.525\text{-}0.733$.[6]

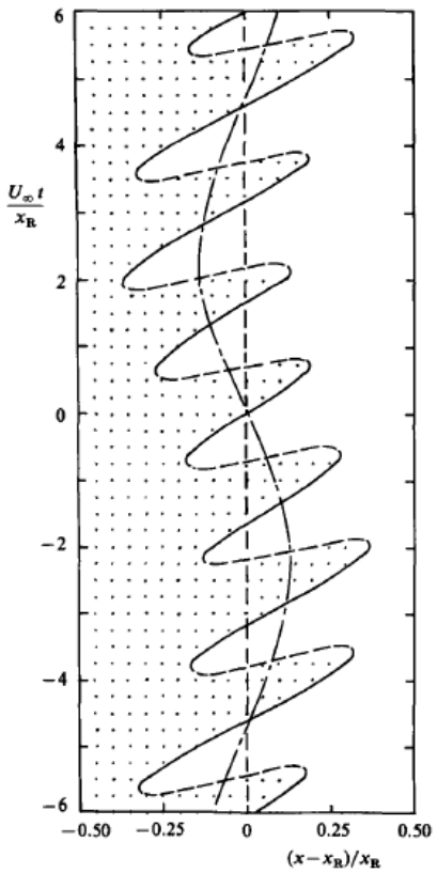

Fig. 2. Schematic of unsteady shear-layer reattachment location, after Kiya and Sasaki.[12] Solid and dashed lines represent contribution from vortical motion, dot-dash lines represent shear-layer flapping contribution.

Flowfield Feature Locations from Hot-Film Array Measurements

Since the low-frequency oscillations in iced-airfoil performance are thought to be linked to the low-frequency "flapping" behavior of the separated shear layer, it is desirable to be capable of determining the unsteady location and frequency content of shear-layer reattachment corresponding to simultaneous measurements of airfoil performance data. In order to accomplish this, a new method for estimating the unsteady shear-layer reattachment location was developed. This method was based on the measurements obtained from a hot-film array mounted over the streamwise zone of shear-layer reattachment on an airfoil with a leading-edge horn-ice shape. The concept behind this method was largely motivated by prior research with hot-film arrays,[19-22] which has led to the discovery that the reattachment location of a separated laminar flow could be determined using surface-mounted hot-film arrays. Stack et al.[23] identified the phenomenon where the location of laminar separation and turbulent reattachment on two airfoils exhibited a reversal in phase between two adjacent sensors of a hot-film array. The use of this phase reversal phenomenon to determine flow reattachment location was later utilized by Lee and Mateescu[22] to determine the mean reattachment location downstream of a backward-facing step.

The use of hot-film arrays in previous investigations to determine flowfield features has not been limited to the phase reversal technique. Olson and Thomas[19] developed a slightly different scheme for measuring the mean reattachment location by using a hot-film array mounted downstream of a backward-facing step. They used the relative shift in the phase spectrum between adjacent sensors to generate a "time of flight" of given Fourier modes at discrete frequencies. The sign of the calculated time of flight between two given sensors was used to determine whether that sensor interval resided upstream or downstream of the mean reattachment location, with zero time of flight corresponding to the mean reattachment location. It was also discovered in this investigation that at the

location of reattachment, there was a decrease in the linear coherence between adjacent sensors over a low-frequency range.

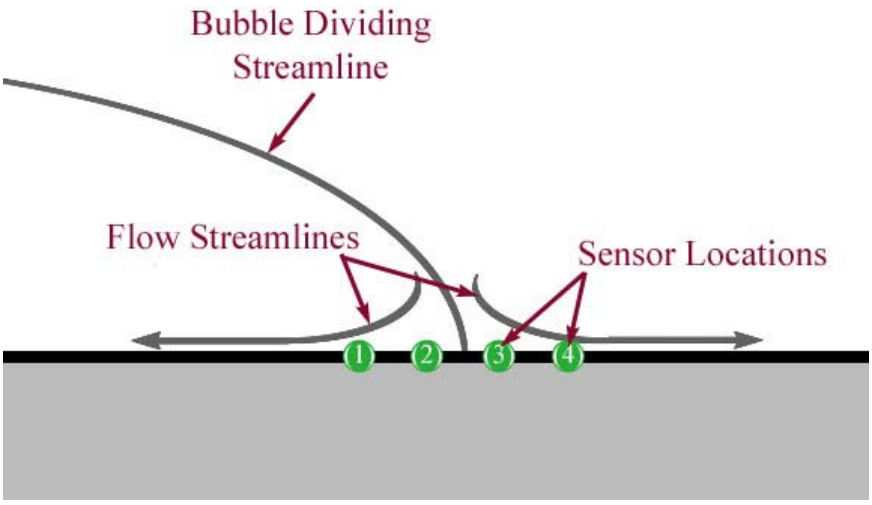

Fig. 3. Schematic of shear layer reattachment on airfoil surface.

The cause of this reversal in the signal phase between adjacent sensors was attributed to the flow bifurcation that occurs at reattachment. When the flow reattaches, both upstream and downstream fluid paths develop, similar to the bifurcation of a planar jet impinging on a flat plate. This causes any flow structures and fluctuations that are being convected by the flow to follow either an upstream or a downstream path. This is shown schematically in Fig. 3. These structures are observed successively as they pass elements of the hot-film array further along the streamline. As a result, there exists a reversal in phase (shift by 180°) between adjacent sensors at the location where flow reattachment occurs.

II. Experimental Methods

Wind Tunnel Data Acquisition

The data obtained in this investigation were acquired from a series of wind tunnel tests, performed at the University of Illinois at Urbana-Champaign on two airfoil models: a single-element NACA 0012 model and an NACA 23012 model with a 25%-chord simple flap. Wind tunnel testing was performed in the Illinois 3-ft × 4-ft low-turbulence, low-speed wind tunnel. The maximum empty test-section speed of this wind tunnel was approximately 165 mph (242 ft/sec), resulting in a maximum Reynolds number of 1.5×10^6/ft with freestream turbulence intensity below 0.1% for all operating speeds. Both airfoil models used in this test had an 18-inch chord. In this investigation, all data were obtained at a chord-based Reynolds number of 1.8×10^6 ($M_\infty = 0.18$). Airfoil lift and pitching moment data were obtained using a three-component balance located below the test section as well as from integrated surface pressures obtained from a series of pressure taps distributed on the model surface and an electronically scanned pressure measurement system. Airfoil drag data were obtained using a traversable wake rake located downstream of the airfoil model.

An array of surface-mounted hot-film probes was also mounted on the upper surfaces of both the NACA 0012 and NACA 23012 models. Separate hot-film arrays were used between the two models. The hot-film array that was installed on the NACA 0012 model consisted of 32 elements and covered a chordwise length from $x/c = 0.39$ to $x/c = 0.57$. The hot-film array that was installed on the NACA 23012 model consisted of 60

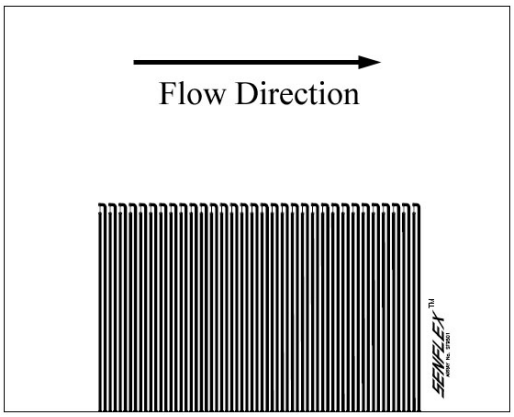

Fig. 4. Diagram of hot-film array used on the surface of the NACA 0012 model, adapted from Ref. 24.

elements and covered a chordwise length from $x/c = 0.1$ to $x/c = 0.425$. A diagram of the hot-film array used on the NACA 0012 model is shown in Fig. 4, after Ref. 24. Each element in the hot-film array was regulated using a dedicated constant-temperature anemometer channel. The hot-film measurements were sampled simultaneously using a National Instruments SCXI scanning system. These unsteady data were acquired at sample rates of 2 kHz on the NACA 0012 and 2.5 kHz on the NACA 23012. Samples were acquired for 10 seconds and were low-pass filtered at the respective Nyquist cutoff frequency using a low-pass Bessel filter.

The NACA 0012 model had a removable leading edge, which provided the capability of testing the model in a clean configuration or an iced configuration. The ice shape that was used in this investigation was the same two-dimensional horn-ice simulation studied by Gurbacki.[6] The original accretion was acquired for 3.5-minutes at 27.5 °F, with liquid water content of 0.55 g/m^3 and mean volumetric diameter of 20-μm. The two-dimensional extrusion was selected over a three-dimensional scaled casting in order to reduce the amount of spanwise variation in the flowfield. A profile of the NACA 0012 with the horn-ice shape is shown in Fig. 5, after Gurbacki.[6] The resulting obstacle height of the horn, measured normal from the airfoil surface, was $k/c = 0.0202$.

Some horn and spanwise-ridge ice shapes can also be simulated using a forward-facing quarter-round geometry. The forward-facing quarter-round has been used in many previously investigations to simulate ice shapes.[25-29] In the current investigation, the ice accretion was simulated on the NACA 23012 model using a forward-facing quarter-round with a 0.25-inch height, corresponding to $k/c = 0.0139$, which was placed on the airfoil upper surface at $x/c = 0.02$. A schematic of the simulated ice on the NACA 23012 model is shown in Fig. 7, after Ansell et al.[9]

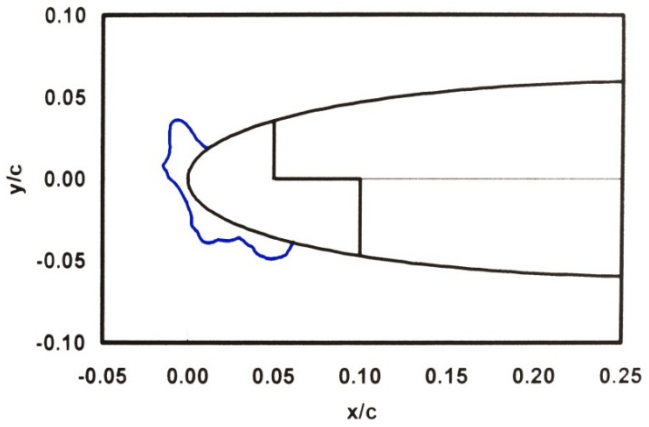

Fig. 5. Schematic of the simulated ice shape on the NACA 0012 model, after Gurbacki.[6]

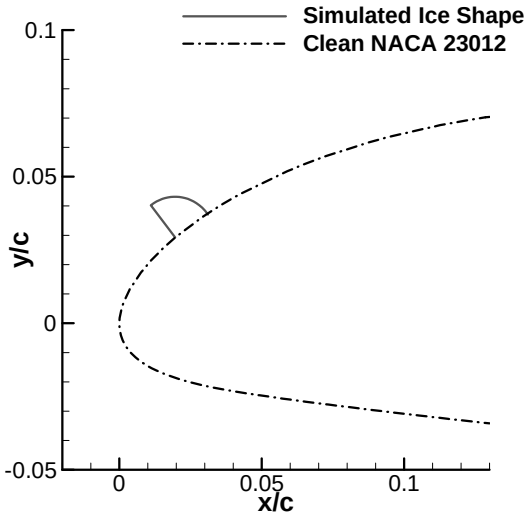

Fig. 6. Schematic of the simulated ice shape on the NACA 23012 model, after Ansell et al.[9]

Statistical Hot-Film Data Reduction

A new method was developed to determine the instantaneous location flow reattachment using the measurements obtained from hot-film arrays. In this investigation, the measurements from the hot-film arrays downstream of the simulated ice shapes were used to determine the unsteady location of shear-layer reattachment. This new method was developed based on the methods of previous investigations where hot-film array measurements were used to determine the mean location of flow reattachment. It was known that when flow reattachment occurs on a hot-film array, there exists a reversal in phase between adjacent sensors corresponding to the reattachment location. In order to determine the instantaneous location of phase reversal between adjacent sensors, the cross-correlation coefficients between adjacent sensor measurements was taken across a short-time sliding window. The cross-correlation coefficient was calculated based on an estimation of the cross-correlation function, which when computed directly can be calculated by[30]

$$\widehat{R}_{pq}(r\Delta t) = \frac{1}{N\text{-}r}\sum_{n=1}^{N\text{-}r} p_n q_{n+r} \tag{1}$$

where N represents the number of data samples, $r = 0, 1, 2, \ldots, m$ represents the given time lag interval (with $m < N$), and p and q represent the quantities for which the cross-correlation is being computed. It should be noted that for this investigation, Δt was known to be the inverse of the sample rate, thus making the quantity $r\Delta t$ the time lag, τ, between points n and $n + r$. Using the calculated cross-correlation function, the cross-correlation coefficient, ρ_{pq}, was estimated using,[30]

$$\hat{\rho}_{pq}(\tau) = \frac{\hat{R}_{pq}(\tau)}{\hat{\sigma}_p \hat{\sigma}_q} \tag{2}$$

where σ represents the standard deviation of the sample. Upon obtaining the series of cross-correlation values, the location of shear-layer reattachment, corresponding to a particular instant, was determined to occur between the adjacent sensors exhibiting the strongest levels of anti-correlation across the corresponding short-time window.

The theory behind this method is similar to the phase reversal method for detecting reattachment location. When imagining a reversal in phase between two sinusoids, the instant in time where one sinusoid would reach a local maximum would correspond to the same instant in time the other sinusoid would reach a local minimum. As a result, the reversal in phase between two signals corresponds to an anti-correlation between these two signals. Also, as described previously, and as shown in Fig. 3, the shear layer reattachment causes streamlines to follow paths upstream and downstream of the reattachment location. This bifurcation causes flow structures or fluctuations to be convected along streamlines in opposing directions. As a result, the fluctuations can be traced through time past the probe elements of the hot-film array. Thus, when calculating the cross-correlation coefficient, adjacent sensors that reside on the same side (upstream or downstream) of the reattachment location will exhibit strong levels of correlation near zero time lag, as the same flow structures are observed by these adjacent sensors successively over a short time lag. When reattachment occurs between two probe elements, the probes do not observe the same flow structures, and the cross-correlation coefficient will exhibit strong levels of anti-correlation near zero time lag. An example of this is shown in Fig. 7.

The cross-correlation coefficients between hot-film sensor elements were calculated across a small time window, and the location corresponding to the maximum anti-correlation between adjacent sensors, nearest to zero time lag, was identified. The position of the time window was then shifted by one measurement in time, and the cross-correlation coefficients and position of maximum anti-correlation were calculated for the new time interval. This process was repeated across the entire time history for all pairs of adjacent sensors. This led to the generation of a locus of points corresponding to the locations across the hot-film array of maximum anti-correlation between adjacent films as a function of time. However, it was possible that some of the estimated reattachment locations were potentially erroneous. In correlation analysis, a value of correlation coefficient between 0 and 0.2 is typically indicative of very weak to negligible correlation. As a result, any reattachment locations that were determined from a correlation coefficient above -0.2 were replaced with the second choice in reattachment location, where the maximum anti-correlation occurred slightly farther from zero time lag, but exhibited a correlation coefficient below -0.2. In order to further minimize the influence of outlying points where the reattachment location may have been incorrectly identified, a short-time moving average of the reattachment location was taken. The result of processing these data was a time history of the reattachment location of the shear layer downstream of the simulated ice shape as a function of time.

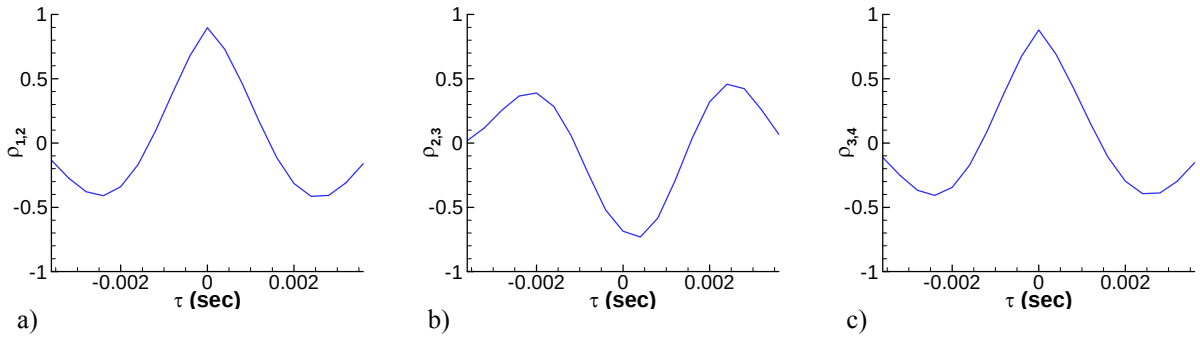

Fig. 7. Example of cross-correlation coefficients between adjacent sensors; sensor numbers shown in Fig. 3: a) upstream of reattachment, b) at reattachment, c) downstream of reattachment.

One of the advantages of using the cross-correlation method for determining flowfield features outlined in this paper is the capability of determining the time-dependent behavior of the reattaching shear layer location. Prior investigations where hot-film arrays were used to distinguish flowfield features were largely focused on using the phase reversal phenomenon to identify the average location of shear-layer reattachment. Averaging is oftentimes required when calculating the phase spectrum between two signals, which makes it difficult to capture the unsteady changes in shear-layer reattachment location over time by observing phase reversals in the phase spectrum. Furthermore, many of the prior investigations where the phase reversal method was used involved a low-speed freestream. Since the current investigation utilized a higher-speed subsonic flow, the separated shear layer and resulting reattachment features occurred with higher levels of energy than the low-speed flows. This made it difficult to determine the exact location of a reversal in phase, since the phase spectrums tended to be noisy, unless many averages were taken. One of the drawbacks of being unable to use the phase spectrum, however, is the inability to calculate the time of flight of a given Fourier mode across the hot-film array. Such a method would be particularly useful in studies like the current investigation, where changes to the local flowfield are attributed to different frequencies. Studying the time of flight of separate Fourier modes that contribute to the overall flowfield unsteadiness would provide additional insight as to how the separate modes develop in time to produce the resulting flowfield in either an independent manner, or through some form of interaction.

IV. Results and Discussion

As the size of the moving average across the reattachment time history was increased, more of the high-frequency content within the reattachment time history was averaged out. In statistics, moving averages are commonly applied to time histories in order to smooth out small time-scale fluctuations in order to better highlight longer time-scale trends. In signal processing, a moving average takes the form of a very simple low-pass filter with finite impulse response.[31] For example, the hot-film data acquired with the NACA 0012 model were sampled at a rate of 2 kHz, so using a moving average of ten samples would have a similar effect as applying a low-pass filter to the data with a cutoff frequency of 200 Hz. As a result, by changing the window size of the moving average, the effects of the regular mode of vortex shedding and the shear-layer flapping on the reattachment location could be observed. Segments of the resulting reattachment location time histories are shown in Fig. 8 for the NACA 0012 airfoil with the leading-edge horn-ice shape at $\alpha = 5°$. Fig. 8 a) shows the small time-scale effect of the regular mode of vortex shedding on the reattachment location, and was generated using a 7-point moving average, which was similar to applying a 285.7 Hz low-pass filter. Fig. 8 b) shows the longer time-scale effect of the shear-layer flapping on the reattachment location and was generated using a 60-point moving average, which was similar to applying a 33.3 Hz low-pass filter.

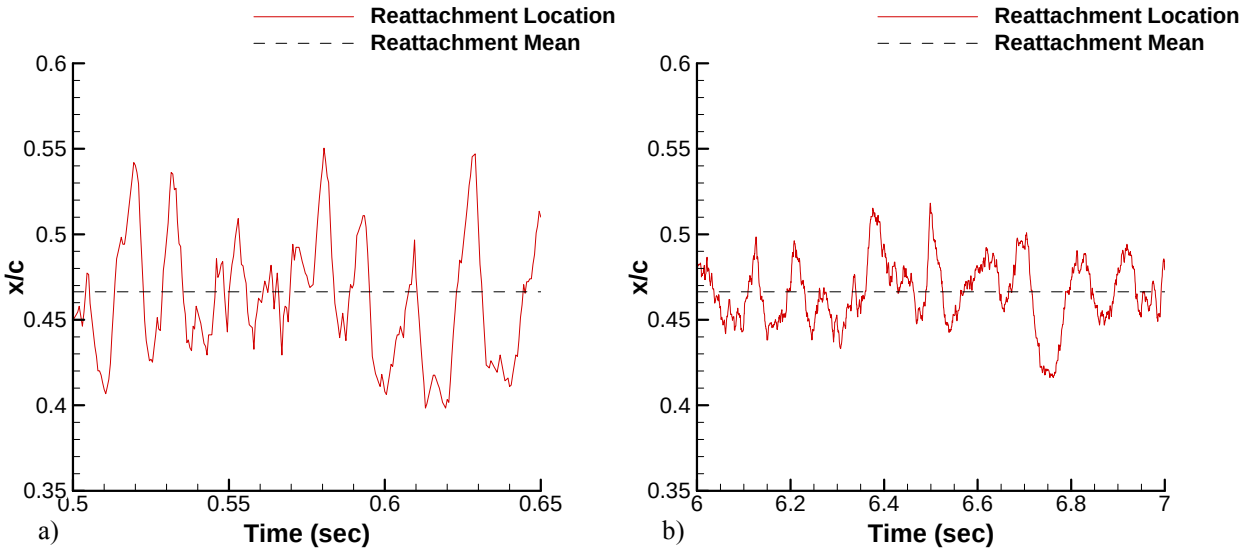

Fig. 8. Time history of unsteady shear-layer reattachment location on the NACA 0012 with a leading-edge horn-ice shape at $\alpha = 5°$: a) determined from 7-point moving average (0.15 seconds shown), b) determined from 60-point moving average (1 second shown).

From Fig. 8 a), the effect of the regular mode of vortex shedding on the reattachment location is characterized by the creation of a sawtooth-wave-like pattern. This pattern is created as the separation bubble grows and undergoes vortex shedding. As vorticity is shed from the reattaching shear layer, the reattachment length exhibits a sharp decrease. After this shedding event, the separation bubble begins to grow, and undergoes another shedding event, leading to a sharp decrease in bubble length. Similar patterns have also been observed by previous researchers studying reattaching shear layers.[32,33]

From Fig. 8 b), the effect of shear-layer flapping on the reattachment location is characterized by a low-frequency, global oscillation in the mean reattachment location. This oscillation is associated with much longer time scales than the regular mode of vortex shedding. The shear-layer flapping component of the reattachment location time history is also consistent with the observations of Kiya and Sasaki,[12] where the low-frequency unsteadiness was represented by a low-frequency oscillation of the local average location of shear-layer reattachment location about the total average location of shear-layer reattachment.

The time-average flowfield characteristics for the NACA 0012 model with the leading-edge horn-ice shape at α = 5° were determined using the surface-oil flow visualization, presented in Fig. 9. By comparing Fig. 9 with Fig. 8, the mean reattachment location determined from the fluorescent-oil flow visualization is consistent with the mean reattachment location determined from the hot-film array. Also shown in Fig. 9 is the approximate boundary of the reattachment zone, indicated by the dashed curves. This boundary was qualitatively determined by marking locations where the oil-flow pattern appeared to change from a strong displacement in a single chordwise direction to a weaker displacement due to reductions in mean shear stress created by the influence of the flow stagnation at reattachment. Like the mean reattachment location, the reattachment zone boundaries appeared to be consistent between fluorescent-oil flow visualization and the locations determined from the hot-film array.

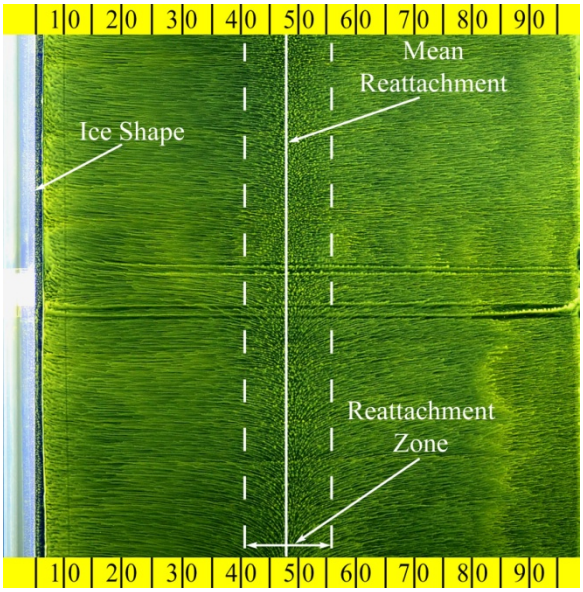

Fig. 9. Time-averaged surface flowfield for NACA 0012 with simulated ice shape at α = 5°.

The unsteady reattachment location was also determined for the NACA 23012 model with the simulated glaze-ice accretion located at x/c = 0.02. The resulting time history is shown in Fig. 10 for α = 6°. Gurbacki showed that for the regular mode of vortex shedding, a Strouhal number scaling dependent on the average length of the separation bubble provided reasonably consistent values.[6] Thus, the frequency of the regular mode tended to scale inversely with the length of the separation bubble for constant freestream velocity. Since the separation bubble was much smaller for the iced-airfoil flowfield of the NACA 23012 at α = 6°, the frequency the regular mode of vortex shedding was significantly higher for the NACA 23012 case. As a result of the limited sampling frequency of the data acquisition system and the high-frequency nature of the regular mode, the effect of the regular mode of vortex shedding on the unsteady reattachment location could not be sufficiently resolved with the moving average window size necessary to capture this phenomenon. However, since the effects of shear-layer flapping occurred at a much lower frequency, these effects could be sufficiently resolved for the NACA 23012 test case. The reattachment time history in Fig. 10 was created using a 75-point moving average, which had a similar effect as applying a 33.3 Hz low-pass filter. From Fig.

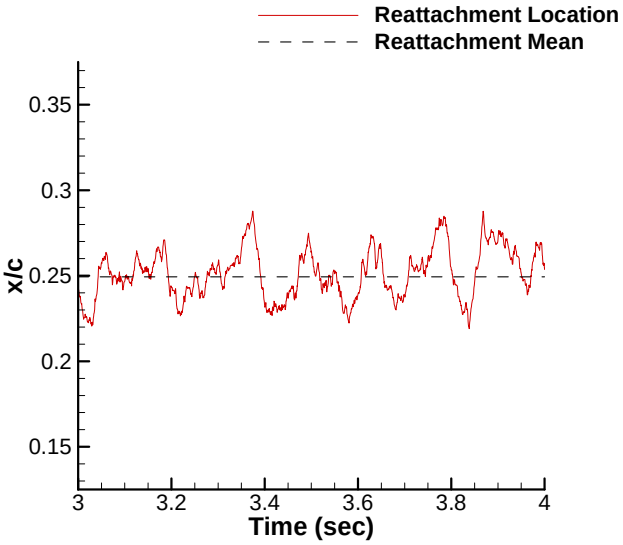

Fig. 10. Time history of unsteady shear-layer reattachment location on the NACA 23012 with a simulated leading-edge ice shape at α = 6°, determined from 75-point moving average.

10, the effect of the shear-layer flapping on the unsteady reattachment location is visible. Like the case for the NACA 0012, the time history in Fig. 10 reveals that the shear-layer flapping component of the unsteady reattachment location is characterized by a low-frequency oscillation of the local average location of shear-layer reattachment about the total average location of shear-layer reattachment.

The time-averaged flowfield characteristics for the NACA 23012 model were also determined using fluorescent-oil flow visualization, as shown in Fig. 11 for α = 6°. As shown in Fig. 11, the mean reattachment location determined from the fluorescent-oil flow visualization at the model mid-span, where the hot-film array was placed, is consistent with the mean reattachment location determined from the hot-film array. It should be noted that there existed some spanwise variation in the reattachment location across the airfoil model due to interference from the test section walls, as can be seen in Fig. 11. Farther from the model mid-span, the mean reattachment location tended to be further downstream than the mean reattachment from the mid-span section. The reattachment zone for the NACA 23012 model iced flowfield was also estimated using a similar method that was used for the NACA 0012 flow visualization results. By comparing this reattachment zone visualized in Fig. 11 to the unsteady location of shear-layer reattachment in Fig. 10, it can be seen that the boundaries of the reattachment zone are also consistent between the fluorescent-oil flow visualization and the locations determined from the hot-film array.

Fig. 11. Time-averaged surface flowfield for NACA 23012 with simulated ice shape at α = 6°.

The behavior of the unsteady location of shear-layer reattachment was further investigated by analyzing the power spectral density (PSD) function of the location of reattachment. When generating this PSD function, the unsteady reattachment location was calculated without the use of a moving average, as this would distort the PSD function in intervals corresponding to the number of time steps included in the moving average. The PSD for the unsteady reattachment location on the NACA 0012 model is shown in Fig. 12 across a low-frequency range. The effect of shear-layer flapping was particularly difficult to analyze, as this phenomenon has been identified as being non-periodic.[18,34] As a result, a great deal of averaging and signal processing must be completed in order to identify the average peaks in the signal energy. From Fig. 12, the low-frequency peak at 8.8 Hz corresponds to the average frequency of the shear-layer flapping phenomenon. The 8.8 Hz peak was selected over the 4 Hz peak, as the 8.8 Hz peak had a wider bandwidth, which would be more representative of a process lacking discrete periodicity. Moreover, the peak at 8.8 Hz corresponded to a Strouhal number that was more consistent with those reported in literature. Using the 8.8 Hz frequency, the Strouhal number of shear-layer flapping, based on the projected height of the airfoil, was calculated to be St_f = 0.00575.

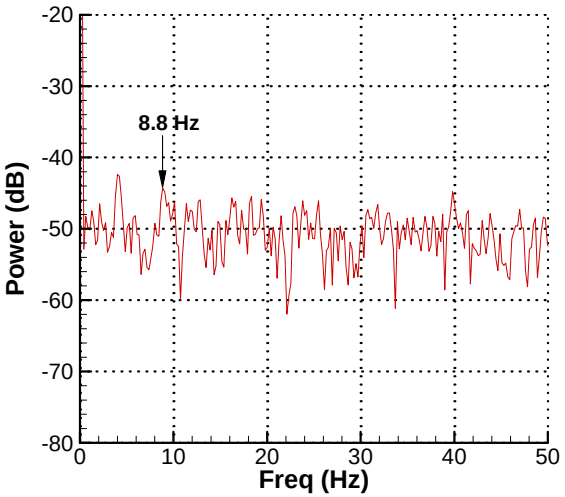

Fig. 12. Low-frequency range of PSD for unsteady shear-layer reattachment location of NACA 0012 with simulated leading-edge horn-ice shape at α = 5°.

The dominant frequencies of the regular mode of vortex shedding were determined using the measurements from a miniature pressure transducer integrated into the NACA 0012 model upper surface at x/c = 0.85. The resulting PSD function for the C_p measurements acquired at this location is shown in Fig. 13 a). Much like with the observations by Gurbacki, the regular mode was observed not to occur at a discrete frequency, but rather across a

broad bandwidth of frequencies.[6] From Fig. 13 a), increases in energy were visible across the frequency range from 90 Hz to 250 Hz, with the peak in energy occurring at 142 Hz. This is consistent with the observations of Ripley and Pauley, where the frequency of vortex shedding was irregular, and the primary shedding frequency tended towards the lower-frequency end of the band of shedding frequencies.[35] Using this peak frequency of 142 Hz, the Strouhal number of the regular mode of vortex shedding, based on the average length of the separation bubble, was calculated to be $St_r = 0.496$.

The PSD function for the reattachment location is also shown in Fig. 13 b) across a high-frequency range. From Fig. 13 b), the contribution of the regular mode of vortex shedding on the unsteady reattachment location is not clearly visible. In Fig. 13 b), the low-frequency content due to shear-layer flapping is dominant over the frequency content for the regular mode of vortex shedding. Since the frequency range of the regular mode resides within the influence of the low-frequency content of the shear-layer flapping, the energy increase due to the regular mode of vortex shedding appears to be obscured by the greater energy content of the shear-layer flapping.

The spectral content of the reattachment location on the NACA 23012 airfoil with simulated leading-edge glaze-ice accretion at $\alpha = 6°$ was also studied. The PSD for this case is shown in Fig. 14, over both the low-frequency range and the full-frequency range tested. From Fig. 14 a), the low-frequency peak at 6 Hz corresponds to the effect of the shear-layer flapping phenomenon on the location of shear-layer reattachment. Using this frequency and the projected height of the airfoil model, the corresponding Strouhal number was calculated to be $St_f = 0.00470$.

The effect of the regular mode of vortex shedding on the unsteady reattachment location on the NACA 23012 model with simulated leading-edge glaze-ice accretion was also studied. The PSD for this case across a high-frequency range is shown in Fig. 14 b). From Fig. 14 b), the effect of the regular mode on the spectral content of the unsteady shear-layer reattachment location is visible across the frequency range from 200 Hz to 425 Hz. By comparing Fig. 14 b) and Fig. 13 b), the effect of the regular mode of vortex shedding is much easier to observe for the NACA 23012 test case than it is for the NACA 0012. This is due to the fact that the frequency range of increased energy due to the regular mode of vortex shedding is sufficiently higher than the frequencies affected by the shear-layer flapping phenomenon, making the energy increase due to the regular mode more apparent away from the greater energy increase due to the shear-layer flapping phenomenon. The average peak attributed to the regular mode of vortex shedding was identified to occur at a frequency of 261 Hz. Using this frequency and the average length of the separation bubble, the Strouhal number was calculated to be $St_r = 0.489$.

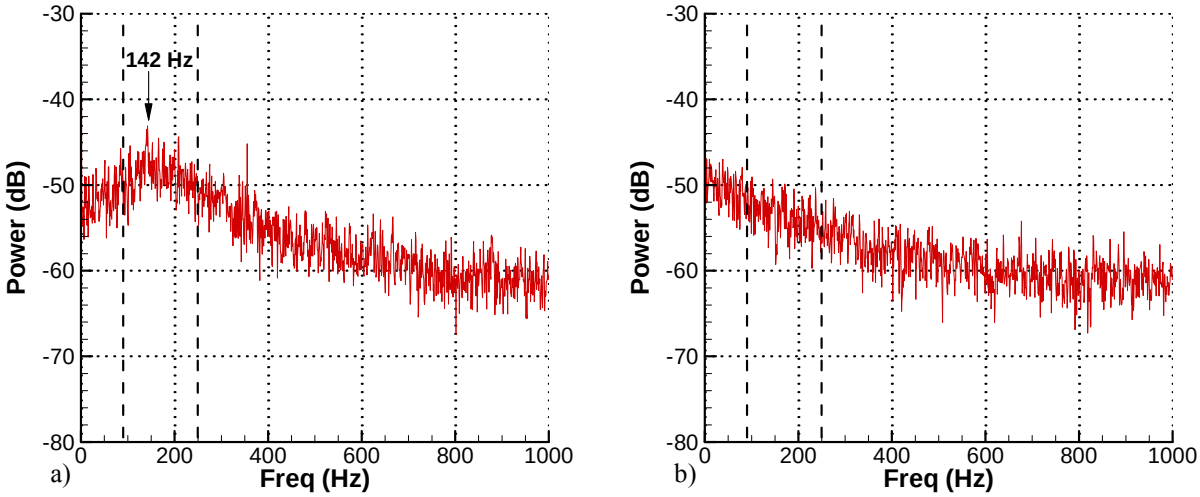

Fig. 13. High-frequency range of PSD for NACA 0012 with leading-edge horn-ice shape at α = 5°: a) unsteady C_p at x/c = 0.85, y/c = 0.021; b) unsteady shear-layer reattachment location.

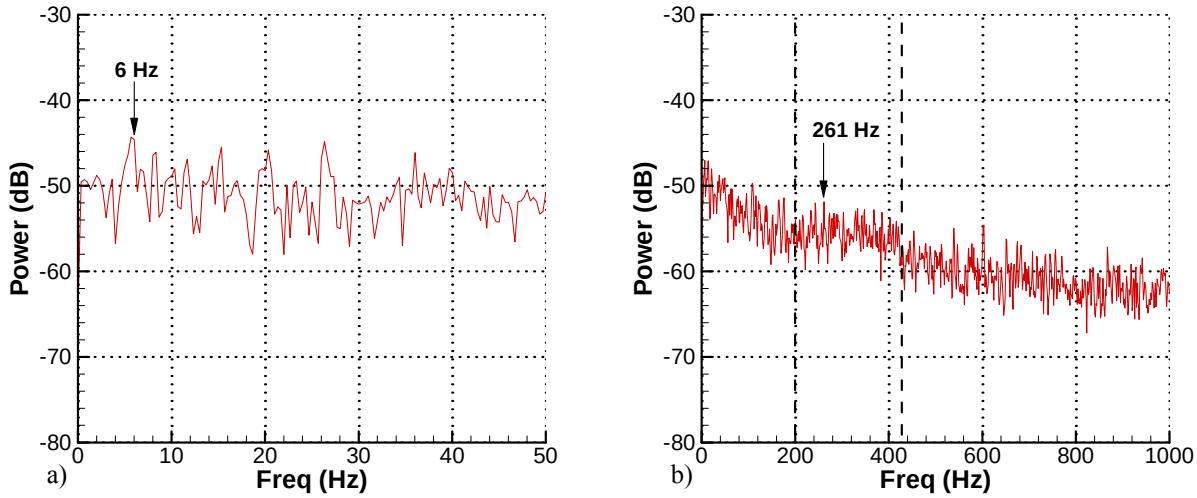

Fig. 14. Unsteady shear-layer reattachment location PSD of NACA 23012 with simulated leading-edge glaze-ice accretion at α = 6°: a) low-frequency range; b) high-frequency range.

Additional information about the unsteady reattachment process can also be obtained from inspection of the probability density (p) and the cumulative distribution (P) functions of the normalized reattachment location ($[x_{MR,i} - x_{MR}] / x_{MR}$), as shown in Fig. 15. The resulting probability functions are also compared to those found from PIV measurements by Jacobs[34] for a separation bubble downstream of a horn-ice shape on an NACA 0012 airfoil tested at Re = 0.9 × 10^6 and M_∞ = 0.2. From Fig. 15 a), the probability density function of the current study on the NACA 0012 airfoil with the leading-edge horn ice shape at α = 5° follows the same trends as the probability density function from Jacobs corresponding to α = 5°, with one exception. The tails of the probability density function from Jacobs are larger than those from the current study, which also causes the probability distribution function in the current study to have slightly higher values closer to the mean reattachment location. However, the physical locations of these tails on the airfoil surface in the current study corresponded to locations outside of the region covered by the hot-film array. As a result, in the current study the probability density function approaches zero at these locations, since measurements to estimate the shear-layer reattachment location could not be made in those regions. This is also the reason why, in Fig. 15 b), the cumulative distribution function of the current entry deviates from the results of Jacobs for α = 5° far from the mean reattachment location.

The probability density and cumulative distribution functions for the current study on the NACA 23012 with the simulated glaze-ice accretion at α = 6° is also shown in Fig. 15. From Fig. 15 a), the probability density function of this case appears to be qualitatively similar to the probability density function reported by Jacobs[34] for the NACA 0012 airfoil with the leading-edge horn-ice shape at α = 5°. Additionally, the tails of the probability density function for the NACA 23012 in the current study appear to follow the same trends as those from Jacobs. Since a larger hot-film array was used on the NACA 23012 model than was used on the NACA 0012 model, the longer chordwise coverage of the airfoil surface allowed the tails of the probability density function to be sufficiently resolved.

The probability density functions reveal that the reattachment location occurs most often near the mean location, and the probability decreases as the location deviates further from the mean. This is also indicated in the cumulative distribution function, where the slopes of the functions are greatest near the mean reattachment location, and taper off with increased distance from the mean. By comparing the probability density and cumulative distribution function from the current study to those from Jacobs,[34] the current method for estimating the unsteady reattachment location using hot-film array measurements is shown to be consistent with the trends in shear-layer reattachment location determined from PIV.

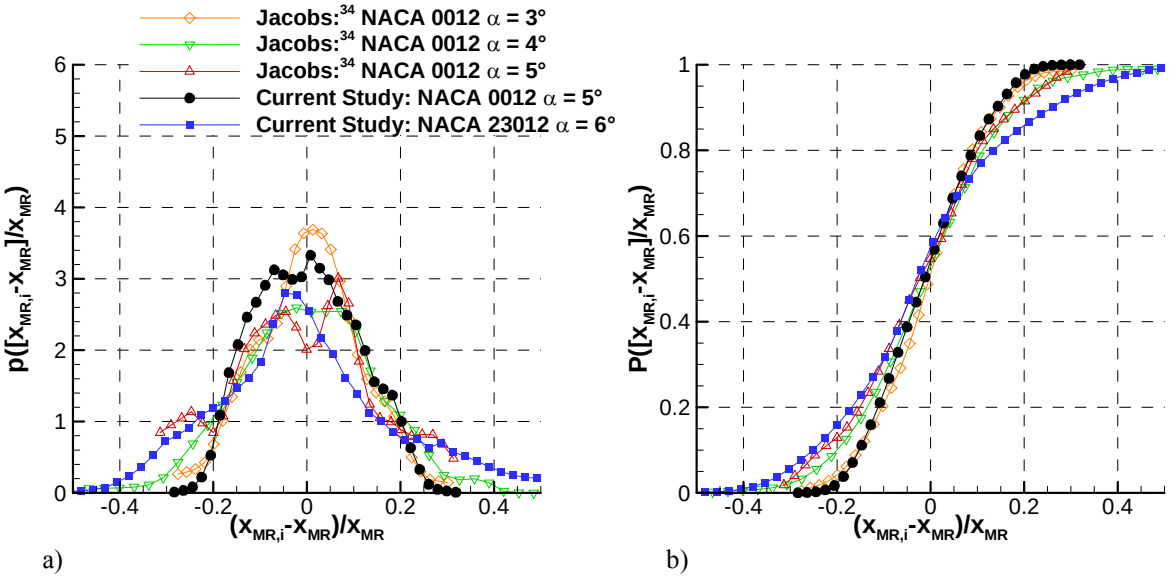

a) b)

Fig. 15. a) Probability density (*p*) and b) cumulative distribution (*P*) functions of the normalized unsteady reattachment location; comparisons provided after Jacobs.[34]

V. Summary and Conclusions

This paper provides an overview of an innovative method for measuring the unsteady shear-layer reattachment location downstream of an ice shape using a surface-mounted hot-film array. This method utilizes strong levels of anti-correlation between adjacent probes to determine the instantaneous location of shear-layer reattachment. Use of this method provided the unsteady reattachment locations on two airfoil models, each with a simulated leading-edge ice shape. The resulting time histories for the unsteady reattachment locations had mean values consistent with those from fluorescent-oil flow visualization. Influences of the regular mode of vortex shedding and shear-layer flapping were visible in the unsteady reattachment location time history. The spectral content of the unsteady reattachment locations also revealed the influences of the regular mode of vortex shedding and shear-layer flapping. The resulting Strouhal numbers corresponding to frequencies of peaks in energy were consistent with values reported in literature. Statistical reduction of the unsteady location of shear-layer reattachment also shows consistencies between the current investigation and results reported in literature.

Acknowledgements

The authors wish to thank Dr. Michael Kerho and Rolling Hills Research Corporation, along with Mark Davis and the staff of NASA Dryden Flight Research Center for their contributions to this work. Support for this program was provided via STTR Contract No. NNX10CB57C.

References

[1] Addy, H.E., Potapczuk, M.G., and Sheldon, D.W., "Modern Airfoil Ice Accretions," AIAA-97-0174, *35th AIAA Aerospace Sciences Meeting and Exhibit*, Reno, NV, Jan. 1997.

[2] Bragg, M.B., Broeren, A.P., and Blumenthal, L., "Iced-Airfoil Aerodynamics," *Progress in Aerospace Sciences*, Vol. 41, No. 5, 2005, pp. 323-362.

[3] Broeren, A.P., Bragg, M.B., Addy, H.E., Lee, S., Moens, F., and Guffond, D., "Effect of High-Fidelity Ice-Accretion Simulations on Full-Scale Airfoil Performance," *AIAA Journal of Aircraft*, Vol. 47, No. 1, 2010, pp. 240-254.

[4] Bragg, M.B., Hutchison, T., Merret, J., Oltman, R., and Pokhariyal, D., "Effect of Ice Accretion on Aircraft Flight Dynamics," AIAA-2000-0360, *38th AIAA Aerospace Sciences Meeting and Exhibit*, Reno, NV, Jan. 2000.

[5] Broeren, A.P., "An Experimental Study of Unsteady Flow Over Airfoils Near Stall," Ph.D. Dissertation, Department of Mechanical and Industrial Engineering, University of Illinois, Urbana, IL 2000.

[6] Gurbacki, H.M., "Ice-Induced Unsteady Flowfield Effects on Airfoil Performance," Ph.D. Dissertation, Department of Aeronautical and Astronautical Engineering, University of Illinois, Urbana, IL 2003.
[7] Bragg, M.B., Khodadoust, A., Spring, S.A., "Measurements in a Leading-Edge Separation Bubble due to a Simulated Airfoil Ice Accretion," *AIAA Journal*, Vol. 30, No. 6, 1986, pp. 1462-1467.
[8] Gurbacki, H.M., and Bragg, M.B., "Unsteady Aerodynamic Measurements on an Iced Airfoil," *42nd AIAA Aerospace Sciences Meeting and Exhibit*, Reno, NV, Jan. 2004.
[9] Ansell, P.J., Bragg, M.B., and Kerho, M.F., "Envelope Protection System for Iced Airfoils Using Flap Hinge Moment," 11ICE-0025/2011-38-0066, *SAE 2011 International Conference on Aircraft and Engine Icing and Ground Deicing*, Chicago, IL, June, 2011.
[10] Eaton, J.K., "Turbulent Flow Reattachment: An Experimental Study of the Flow and Structure Behind a Backward-Facing Step," Ph.D. Dissertation, Stanford University, 1980.
[11] Driver, D.M., Seegmiller, H.L., and Marvin, J., "Unsteady Behavior of a Reattaching Shear Layer," *AIAA 16th Fluid and Plasma Dynamics Conference*, Danvers, MA, July, 1983.
[12] Kiya, M., and Sasaki, K., "Structure of Large-Scale Vortices and Unsteady Reverse Flow in the Reattaching Zone of a Turbulent Separation Bubble," *Journal of Fluid Mechanics*, Vol. 154, 1985, pp. 463-491.
[13] Spazzini, P.G., Iuso, G., Onorato, M., Zurlo, N., and Di Cicca, G.M., "Unsteady Behavior of Backward-Facing Step Flow," *Experiments in Fluids*, Vol. 30, 2001, pp. 551-561.
[14] Li, Y., and Naguib, A.M., "High-Frequency Oscillating-Hot-Wire Sensor for Near-Wall Diagnostics in Separated Flows," *AIAA Journal*, Vol. 43, No. 3, 2005, pp. 520-529.
[15] Kiya, M., Shimizu, M., and Mochizuki, O., "Sinusoidal Forcing of a Turbulent Separation Bubble," *Journal of Fluid Mechanics*, Vol. 342, 1997, pp. 119-139.
[16] Lee, I., and Sung, H.J., "Multiple-Arrayed Pressure Measurement for Investigation of the Unsteady Flow Structure of a Reattaching Shear Layer," *Journal of Fluid Mechanics*, Vol. 463, 2002, pp. 377-402.
[17] Sigurdson, L.W., "The Structure and Control of a Turbulent Reattaching Flow," *Journal of Fluid Mechanics*, Vol. 298, 1995, pp. 139-165.
[18] Eaton, J.K., and Johnston, J.P., "Low-frequency Unsteadyness of a Reattaching Turbulent Shear Layer," *Turbulent Shear Flows III*, Third International Symposium on Turbulent Shear Flows, University of California at Davis, September, 1981, pp. 162-170.
[19] Olson, S.D., and Thomas, F.O., "Quantitative Detection of Turbulent Reattachment Using a Surface Mounted Hot-Film Array," *Experiments in Fluids*, Vol. 37, 2004, pp. 75-79.
[20] Mangalam, A.S., and Moes, T.R., "Real-Time Unsteady Loads Measurements Using Hot-Film Sensors," NASA/TM-2004-212854, August 2004.
[21] Stack, J.P., Mangalam, S.M., and Kalburgi, V., "The Phase Reversal Phenomenon at Flow Separation and Reattachment," AIAA-88-0408, *AIAA 26th Aerospace Sciences Meeting*, Reno, NV, January 1988.
[22] Lee, T., and Mateescu, D., "Experimental and Numerical Investigation of 2-D Backward-Facing Step Flow," *Journal of Fluids and Structures*, Vol. 12, 1998, pp. 703-716.
[23] Stack, J.P., Mangalam, S.M., and Berry, S.A., "A Unique Measurement Technique to Study Laminar-Separation Bubble Characteristics on an Airfoil," AIAA-87-1271, *AIAA 19th Fluid Dynamics, Plasma Dynamics, and Lasers Conference*, Honolulu, HI, June 1987.
[24] *Senflex Multi-Element Surface Hot-Film Sensors: General Information and Catalog of Standard Arrays*, Tao of Systems Integration, Inc., Hampton, VA.
[25] Lee, S., Bragg M.B., "Experimental Investigation of Simulated Large-Droplet Ice Shapes on Airfoil Aerodynamics," *AIAA Journal of Aircraft,* Vol. 36, No. 5, 1999, pp. 844-855.
[26] Broeren, A.P., Whalen, E.A., Busch, G.T., and Bragg, M.B., "Aerodynamic Simulation of Runback Ice Accretion," AIAA-2009-4261, *1st AIAA Atmospheric and Space Environments Conference,* San Antonio, TX, June 2009.
[27] Lu, B., Bragg M.B., "Airfoil Drag Measurements with Simulated Leading-Edge Ice Using the Wake Survey Method," AIAA-2003-1094, *41st Aerospace Sciences Meeting and Exhibit,* Reno, NV, Jan. 2003.
[28] Gurbacki, H.M. and Bragg, M.B., "Sensing Aircraft Effects by Flap Hinge Moment Measurements," AIAA-99-3149, *17th Applied Aerodynamics Conference,* Norfolk, VA, Jun. 1999.
[29] Ansell, P.J., Bragg, M.B., and Kerho, M.F., "Stall Warning Using Flap Hinge Moment Measurements," *AIAA Journal of Aircraft*, Vol. 48, No. 5, 2011.
[30] Bendat, J.S., and Piersol, A.G., *Random Data: Analysis and Measurement Procedures*, 3rd ed., New York, NY: Wiley-Interscience, 2000, Chapter 11.

[31] Strang, G., and Nguyen, T., *Wavelets and Filter Banks*, 2nd ed., Wellesley, MA: Wellesley-Cambridge Press, 1997, Chapter 1.
[32] Lee, I., and Sung, H.J., "Multiple-Arrayed Pressure Measurement for Investigation of the Unsteady Flow Structure of a Reattaching Shear Layer," *Journal of Fluid Mechanics*, Vol. 463, 2002, pp. 377-402.
[33] Schäfer, F., Breuer, M., and Durst, F., "The Dynamics of the Transitional Flow over a Backward-Facing Step," *Journal of Fluid Mechanics*, Vol. 623, 2009, pp. 85-119.
[34] Jacobs, J.J., "Iced Airfoil Separation Bubble Measurements by Particle Image Velocimetry," Ph.D. Dissertation, Department of Aerospace Engineering, University of Illinois, Urbana, IL 2007.
[35] Ripley, M.D., and Pauley, L.L., "The Unsteady Structure of Two-Dimensional Steady Laminar Separation," *Physics of Fluids A*, Vol. 5, 1993, pp. 3099-3106.